



A scaling law for the length of granular jumps down smooth inclines

Andrés Escobar^{1,2}, François Guillard², Itai Einav² and Thierry Faug^{1,†}

¹Université Grenoble Alpes, CNRS, INRAE, IRD, Grenoble INP[‡], IGE, 38000 Grenoble, France

²School of Civil Engineering, The University of Sydney, Sydney, NSW 2006, Australia

(Received 19 June 2023; revised 8 August 2023; accepted 8 September 2023)

Granular jumps commonly develop during granular flows over complex topographies or when hitting retaining structures. While this process has been well-studied for hydraulic flows, in granular flows such jumps remain to be fully explored, given the role of interparticle friction. Predicting the length of granular jumps is a challenging question, relevant to the design of protection dams against avalanches. In this study, we investigate the canonical case of standing jumps formed in granular flows down smooth inclines using extensive numerical simulations based on the discrete element method. We consider both two- and three-dimensional configurations and vary the chute bottom friction to account for the crucial interplay between the sliding along the smooth bottom and the shearing across the granular bulk above. By doing so, we derived a robust scaling law for the jump length that is valid over a wide range of Froude numbers and takes into account the influence of the packing density. The findings have potential implications on a number of situations encountered in industry as well as problems associated with natural hazards.

Key words: dry granular material, rheology, channel flow

1. Introduction

Rapid mass movements, such as snow avalanches, landslides and debris flows, are common in mountain regions. One shared feature of these flows is their granular nature. Commonly, these flows may also be destructive, posing severe hazards to human lives and infrastructures. A usual way to reduce their catastrophic potential is to consider building structures aimed at slowing down the flow and diverting it (Pudasaini *et al.* 2007; Johannesson *et al.* 2009; Sovilla *et al.* 2012; Iverson, George & Logan 2016; Albaba, Lambert & Faug 2018). When the granular flow hits such structures, the velocity of the granular mass decreases, and the flow thickens and becomes denser. This transition from a

[†] Email address for correspondence: thierry.faug@inrae.fr

[‡] Institute of Engineering and Management Université Grenoble Alpes.

fast, thin flow into a slow thicker one is known as a jump (Gray, Tai & Noelle 2003). In this process, the final, steady-state flow height is critical for designing protective structures.

Granular jumps tend to form when flowing granular materials meet sharp changes in the slope along their path, such as along natural topographies above which avalanches and landslides propagate. A most prominent example for sharp changes causing such jumps occurs when the slopes transition from initial steep sections into run-out zones with lower inclinations (Tai & Lin 2008) or bump-like obstacles (Viroulet *et al.* 2017). Granular jumps also develop in various industrial settings involving the transportation of particles in silos, pipes or chutes (Samadani, Mahadevan & Kudrolli 2002; Jaworski & Dyakowski 2007; Xiao *et al.* 2018). Understanding granular jumps is crucial for mitigating the associated risks and optimizing their industrial applications. An initial approach for their understanding considers an incompressible flow as proposed by Chanson (2009). While this approach may be suitable for nearly subcritical flows, compressibility becomes relevant with increasing velocity, where incoming flows become considerably diluted, bringing a substantial increase in density through the jump. Later studies on granular jumps have demonstrated that the length of compressible jumps is relevant due to energy dissipation from both short-lived collisions and long-enduring frictional contacts between the particles and the base (Méjean, Faug & Einav 2017).

Considering the relevance of friction in granular jumps, this study presents a detailed numerical analysis of the jump length over a wide range of incoming flow conditions, focusing on the effect of slope bottom friction and interparticle friction. The numerical set-up presented here considers two-dimensional (2-D) and three-dimensional (3-D) flows down smooth inclines, which impact a wall located at the end of a chute, thus forming upon impact a jump that travels upstream. During this process, the opening height of an outgoing gate located at the end of the chute is adjusted, aiming to equalize the incoming and outgoing flow fluxes. By doing so, the jump is tuned to remain stationary at a fixed position along the chute. Under such steady-state conditions, the jump is defined as a standing jump, allowing its properties to be averaged in time for effective analysis and interpretation of the physical parameters determining its length.

In order to deliver the last point, the paper is organized as follows: in § 2, we describe the numerical set-up and procedures. In § 3, we present the obtained results, which focus on the main physics of the incoming flow. Next, we examine the jump length measurements. In § 4, we introduce a scaling law for the jump length and discuss its implications. Finally, in § 5, we summarize our results and draw the main conclusions.

2. Methods

2.1. Numerical set-up

Standing granular jumps are simulated with the discrete element method (DEM) using the open-source software YADE (Smilauer 2021). These simulations involve spherical grains of diameter d whose interactions are being controlled by a viscoelastic contact model for the normal forces and an elastic force limited by a Coulomb friction threshold for tangential forces, as proposed by Pournin, Liebling & Mocellin (2001). The normal viscoelastic force is controlled by a linear spring proportional to the normal overlap between grains with stiffness $k_n = Ed/2$ and a dashpot defined by a damping coefficient. The constant E is set to 1×10^6 and 1×10^7 Pa for 2-D and 3-D simulations, respectively, with a typical range of 10^{-3} – 10^{-4} for the maximum values of the ratio of the overlap to the grain diameter. Similarly, the damping coefficient is determined by the grains' restitution coefficient e , which was set as 0.5. Poisson's ratio ν was taken equal to 0.3,

Length of granular jumps down inclines

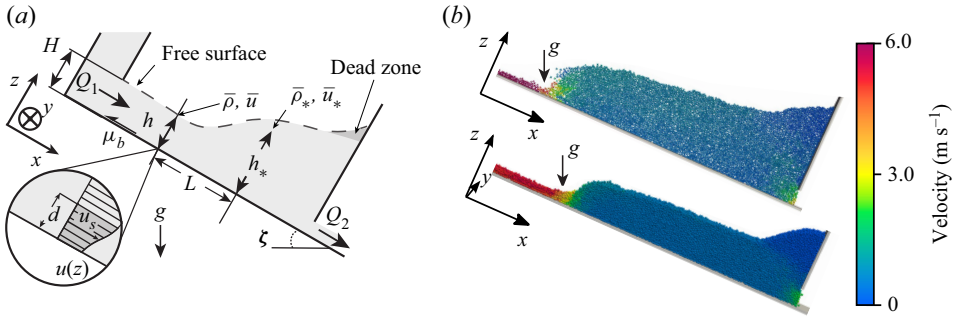


Figure 1. (a) Sketch of a typical simulated granular jump. The circular-shaped inset shows the velocity profile $u(z)$ close to the smooth bottom with slip velocity u_s , as systematically observed in figure 2. (b) Snapshots from 2-D (top) and 3-D (bottom) DEM simulations. Examples with $\zeta = 24$ deg, $H/d = 10$, $\mu_b = 0.24$, $\mu = 0.54$, $d = 4$ cm. In all panels, g refers to gravity acceleration $g = 9.81$ m s⁻².

leading to a tangential stiffness $k_t = \nu k_n$. The material density of the grains ρ_p was defined at 2500 kg m⁻³ to mimic glass beads typically used in experimental works. Time step dt was set as 3×10^{-4} s for the 2-D simulations and decreased to 3×10^{-5} s for the 3-D simulations, following the suggested values by O'Sullivan & Bray (2004). The grains are spherical and their mean diameter d was set as 4 cm with a size distribution of $\pm 15\%d$ to avoid crystallization effects. A few additional simulations were performed using mean diameters of 2 and 6 cm to explore the possible influence of the grain diameter on the jump. The friction along the bottom of the chute was set based on the coefficient μ_b ranging from 0.0315 to 0.72. The grains' internal friction coefficient μ was varied between 0.25 and 0.72. The combination of these friction coefficients was selected so that their ratio would follow $\mu/\mu_b \leq 1$. Finally, the flume inclination angle ζ varied from 8.5 to 48 degrees. The simulation set-up follows a similar one used by Méjean *et al.* (2020), as depicted in figure 1. Two-dimensional simulations were performed using spheres (instead of disks) aligned to the y -axis with their respective rotations and displacement degrees of freedom restricted around this axis. In the 3-D case, periodic boundaries (also known to set so-called 'unconfined flows') were implemented normal to the flow direction (y -axis in figure 1) with a distance (width) between them of $10d$. The gate opening height H , which controls the mass discharge, was set at $H/d = 10, 15$ and 20 . The measurements of both the incoming and outgoing flow fluxes (Q_1 and Q_2) were performed every 30 time steps (see details in § 2.2). Here Q_1 was measured by counting the grains leaving the reservoir, while an equivalent number of grains were added on top of the reservoir in order to ensure it remained full. Similarly, Q_2 was measured by counting the grains that passed through the outgoing gate during the same time period, while these counted grains were removed from the simulation.

2.2. Numerical procedure

Standing jumps are generated by releasing grains from the tank and controlling the outgoing flow at the bottom of the chute. Initially, the reservoir is filled with grains to a height of at least $3H$. In the second, phase the reservoir gate gets opened while the outgoing gate is being closed ($Q_1 \neq 0, Q_2 = 0$). During this phase, the bulk of the grains starts flowing down the chute and later hits the initially closed outgoing gate. In this process, a travelling wave known as a granular bore (Gray & Hutter 1997; Albaba *et al.* 2018) forms. As the bore gets approximately to the centre of the chute, the outgoing gate

is opened to let the grains release from the bottom of the chute. In the next phase, the height of the outgoing gate is adjusted up and down until a steady state is being reached so that the bore's position remains stationary, thus forming what is known as a standing granular jump (see examples depicted in [figure 1](#)). We define the steady state to denote events where the average value of both Q_2 and Q_1 over the last five measurements falls within a 15% tolerance of each other. Once this steady state is achieved, we record the coordinates and velocities of all grains, at least 10 times, with a gap of 0.3 seconds between each recording. This rate of recordings was empirically found to provide a sufficiently smooth signal to properly study and define the steady-state jump. A greater number of recordings was used on certain simulations, but little difference was observed. In order to achieve a smooth signal, we implemented the coarse-graining procedure from Hoover & Hoover (2006) to measure the fields of volume fractions and mean velocities. This coarse-graining was performed using spatial windowing based on Lucy polynomials on a uniformly distributed grid with a spacing of $0.25d$ between nodes. Each node's calculation considered the spheres within a radius of $2.5d$ from that node, based on the previous 2-D numerical study and sensitivity analysis in Méjean *et al.* (2020). Given that in the 3-D simulations the flows are found to be homogeneous across the flume width due to the periodic boundaries, in those simulations the coarse-graining was performed only at the centre of the chute along the x -axis. The free-surface height along the chute $h(x)$ was defined from the coarse-grained solid fraction ϕ field using a limit value ϕ_{lim} used to indicate the transition from liquid to the gaseous regime. The value of ϕ_{lim} was set at 0.15 for 2-D simulations, as defined by Méjean *et al.* (2020). For 3-D simulations, ϕ_{lim} was adjusted to 0.11 in proportion to the difference between the random close packing values measured from the simulations: 0.83 and 0.64 for the 2-D and 3-D cases, respectively. After the free surface is defined, data are depth-averaged to obtain velocity magnitudes and volume fractions along the x direction, denoted as $\bar{u}(x)$ and $\bar{\phi}(x)$, respectively. These depth-averaged signals are smoothed using a 2nd-order Butterworth filter (Selesnick & Burrus 1998) with a critical lowpass frequency of 0.06 m^{-1} . The filter is adjusted to provide the smoothest signal while maintaining the positions of any peaks in the signal. The jump length L is measured based on $\bar{u}(x)$ and its derivative with respect to the x -axis ($d\bar{u}(x)/dx$). The jump produces an abrupt drop in the velocity, as seen in [figure 1\(b\)](#). This drop in velocity is then used to determine the jump limits. The jump starts at the position where the flow begins to decelerate across the chute after leaving the tank ($d\bar{u}(x)/dx = 0$). Considering this identified position, we measure the depth-averaged volume fraction and velocity for the jump ($\bar{\phi}$ and \bar{u} respectively). The depth-averaged jump density $\bar{\rho}$ at the start of the jump is defined as $\bar{\rho} = \bar{\phi}\rho_p$. The end of the jump is identified by analysing the variation of $d\bar{u}(x)/dx$ through the Matlab function *findchangepts()*, which is used to detect the end of the abrupt change produced by the jump. Flow variables at the end of the jump are denoted with the subscript $*$ (see [figure 1](#)). A spreadsheet of all these results is available from the supplementary data available at <https://doi.org/10.1017/jfm.2023.757>.

2.3. Froude numbers

In the following, we present results in terms of dimensionless groups. In former studies about granular jumps, by analogy to hydraulic jumps, the Froude number is commonly defined as

$$Fr(x) = \bar{u}(x) / \sqrt{gh(x) \cos \zeta}. \quad (2.1)$$

Length of granular jumps down inclines

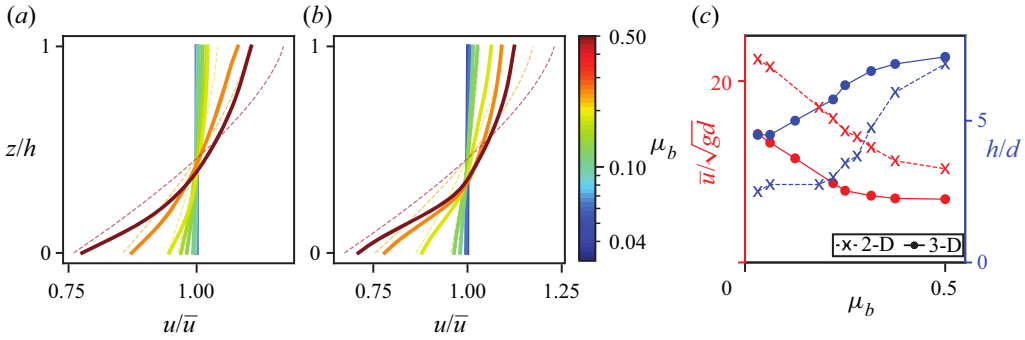


Figure 2. Influence of μ_b on velocity profiles at jump start for 2-D (a) and 3-D (b) simulations. Dashed lines in (a,b) refer to the Bagnold profile best fit. (c) Influence of μ_b on \bar{u}/\sqrt{gd} and h/d . Examples for $\zeta = 24$ deg, $d = 4$ cm, $\mu = 0.54$ and $H/d = 15$.

However, for the present work, the Froude number will be defined as

$$\mathcal{F}(x) = \bar{u}(x)/\sqrt{gh(x)\bar{\phi}(x)\cos\zeta}. \quad (2.2)$$

In the above definition, the depth-averaged volume fraction is considered as we found that it improves the correlation between the measured jump length and the corresponding Froude number in § 3.2 (see figure 3). This slight modification of the Froude number is consistent with previous studies that rely on the depth-integrated volume fraction $\int_0^\infty \phi(z) dz = h\bar{\phi}$, called the mass hold-up (Louge & Keast 2001; Zhu, Delannay & Valance 2020), for granular flows down a smooth bottom. Note that in the present study, the integral is bounded by the flow height, defined from ϕ_{lim} . In addition to \mathcal{F} above, it is found useful to define another Froude number, this time corresponding to the base of the flow:

$$\mathcal{F}_s(x) = u_s(x)/\sqrt{gd\cos\zeta}, \quad (2.3)$$

where u_s refers to the slip velocity on the base, defined as the averaged velocity over one grain diameter distance from the bottom, as sketched in the circular-shaped inset of figure 1. Here \mathcal{F}_s is proposed in addition to \mathcal{F} so that we could account for the sliding at the smooth bottom and its interplay with the bulk deformation across the entire flow thickness.

3. Results

3.1. Incoming flow

In the simulations, the incoming flow does not appear to be affected by the jump. This can be understood due to the supercritical nature ($\mathcal{F} > 1$) of the flow, which moves faster than the downstream influence of the jump can propagate upstream. Additionally, as described in Méjean *et al.* (2020), the simulations show that the detectable rise in the free surface produced by the jump only occurs downstream, after the jump start. Velocity profiles at the position across the flume where the jump starts are strongly influenced by μ_b when all the other parameters remain unchanged, as seen in figure 2(a,b). Furthermore, a theoretical Bagnold profile with slip at the base is shown to fit well the incoming flow profiles, especially in the 2-D simulations where the fit remains good even for high μ_b (see figure 2a).

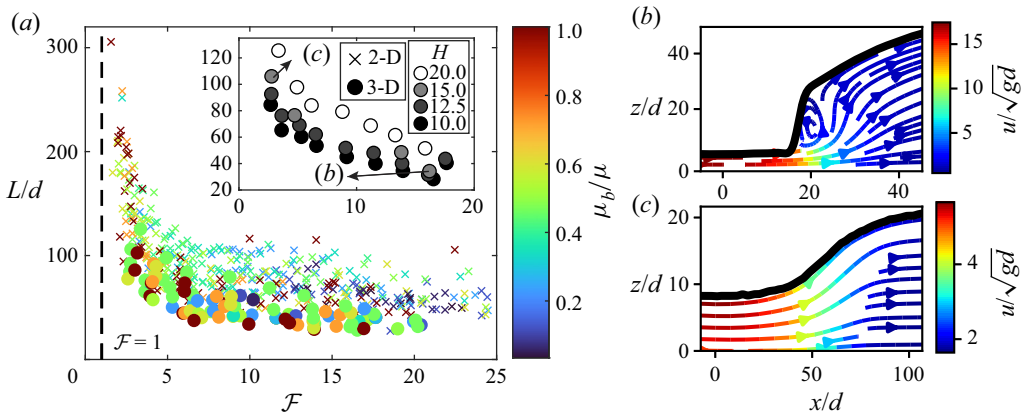


Figure 3. (a) Normalized jump length L/d vs Froude number \mathcal{F} for different μ_b/μ . In inset: an example for all 3-D periodic jumps for different opening heights of the tank ($\mu_b = 0.25$, $\mu = 0.54$). Panels (b,c) show the streamlines for two extreme jumps (data shown in inset of (a)): steep jump with recirculation (b) and laminar jump (c).

All velocity profiles show some level of sliding at the base of the flow. These profiles show a transition from purely plug-like shallow flows ($u_s/\bar{u} = 1$) for low μ_b to thicker sheared flows, yet still with a significant sliding at the base for high μ_b . These normalized plots highlight the transition between plug-like flows that are essentially controlled by the slip velocity at the bottom and flows that still slip significantly but with a well-established shear profile that develops across the bulk when increasing μ_b . Moreover, as illustrated in figure 2(c), an increase in μ_b leads to a decrease in the incoming velocity of the flows while simultaneously increasing the flow height, a trend observed in both 2-D and 3-D simulations.

3.2. Jump length

Figure 3(a) shows the dependence of the normalized jump length L/d on the Froude's number \mathcal{F} at jump start. Upon the normalization of L by d the results generally collapse independently to grain diameter d . On the contrary, the results are more scattered for different flow heights observed in the inset of figure 3(a). Varying μ_b and μ also contributes to the scatter of the data observed in figure 3(a). In spite of that scattering, this figure also displays two important asymptotic regimes in terms of jump length. The first asymptotic regime takes place at high \mathcal{F} values, where the jump length tends to a constant value, which is approximately $50d$ in our numerical simulations. In this regime, steep colliding jumps occur (see figure 3b), as named by Méjean *et al.* (2020). The second asymptotic regime appears when \mathcal{F} approaches the critical flow state ($\mathcal{F} \approx 1$), where L/d diverges, meaning a regime with very elongated jumps. These jumps possess a ‘laminar’ shape (see figure 3c) based on descriptions and terminology in Méjean *et al.* (2020). This shape will ultimately elongate until no jump occurs. The transition between laminar and steep colliding jumps identified in previous experimental studies (Gray *et al.* 2003; Faug *et al.* 2015) remains blurry, which possibly explains the observed scattering in L/d on figure 3(a). This scattering will be resolved in the next section. Finally, it is worth noticing that 3-D jumps have a shorter length than 2-D jumps with similar \mathcal{F} of the incoming flow. This point will be further discussed in the next section.

4. Discussion

4.1. A scaling law for the jump length

The scattering on [figure 3\(a\)](#) is significantly reduced when normalizing L/d by the basal Froude number \mathcal{F}_s , as shown in [figure 4](#). The obtained results show a strong collapse, and thus it could be concluded that it is crucial to account for the sliding at the smooth bottom. The results can be fitted through the function $L/(d\mathcal{F}_s) = \alpha/(\mathcal{F} - 1)$ (thus ensuring that L diverges when \mathcal{F} reaches unity) which can be further expressed as

$$\frac{L}{d} = \alpha \frac{\mathcal{F}_s}{\mathcal{F} - 1} = \alpha \sqrt{\frac{h\bar{\phi}}{d}} \frac{u_s}{\bar{u}} \frac{\mathcal{F}}{\mathcal{F} - 1}, \quad (4.1)$$

where α is a parameter that depends on the system dimension (see obtained values for 2-D and 3-D systems in the inset legend of [figure 4](#)). Scaling using Fr was also considered but led to a poorer collapse of the data. The proposed fit above allows us to describe the jump length in a way that relies only on the depth-averaged flow properties (\bar{u} and $\bar{\phi}$), height h and the sliding velocity u_s , regardless of the previously described scattering produced by both the bottom friction μ_b and the opening height H of the tank, but accounting for the crucial interplay between the amount of sliding at the bottom and shearing across the granular bulk above. Regarding the regime described earlier in [§ 3.2](#), where L diverges when the input condition approaches the critical state ($\mathcal{F} \approx 1$) as seen in [figure 3\(a\)](#), the proposed scaling in [\(4.1\)](#) takes into account the decrease in u_s as seen in [figure 4](#), which helps to maintain the divergence of L . This behaviour is consistent because when the incoming flow approaches subcritical conditions, the sliding at the bottom may vanish while the jump extends over the whole length of the chute. When this occurs, it is less easy for the grains to cross the jump, and the already laminar jump becomes even more diffused. An (extreme) virtual situation occurs when the jump extends over the total length of the chute, which requires the incoming and the outgoing flow fluxes to be the same (subcritical condition reached everywhere). In the other asymptotic regime, the jumps become steeper as the \mathcal{F} value increases, resulting in a higher h_*/h ratio. Steeper jumps resemble those obtained in Pudasaini *et al.* (2007) and Méjean *et al.* (2020). Recirculation starts to appear as a transition towards a fully steep colliding jump (refer to [figure 3b](#)), also consistent with the definition provided by Méjean *et al.* (2020). Although improved relative to [figure 3](#) there are still some differences between the 2-D and the 3-D simulations in [figure 4](#). Specifically, the 3-D jumps are shorter (lower $L/d\mathcal{F}_s$) than the 2-D jumps for the measured values of \mathcal{F} , suggesting that macroscopic friction is higher in 3-D than in 2-D for similar \mathcal{F} . In other systems (e.g. h_{stop} curves for granular flows down rough inclines (GDRMidi 2004), run-out distance in granular column collapse (Utili, Zhao & Houlsby 2015)), macroscopic friction is also generally higher in 3-D than in 2-D. In this context, the jump length represents a proxy to the availability of the granular material to dissipate energy. Shorter jumps mean more dissipative granular bulks compared with longer jumps.

4.2. Bottom slip velocity and improved scaling for jump length

Although the jump length can already be expressed through [\(4.1\)](#), the sliding velocity is not considered in the jump framework proposed by Méjean *et al.* (2017). Moreover, u_s can be challenging to estimate when considering specific geophysical flows. A relationship between the sliding velocity and the depth-averaged velocity is thus proposed:

$$u_s = \beta \bar{u} \left(\frac{d}{h} \bar{\phi} \right)^{0.1}, \quad (4.2)$$

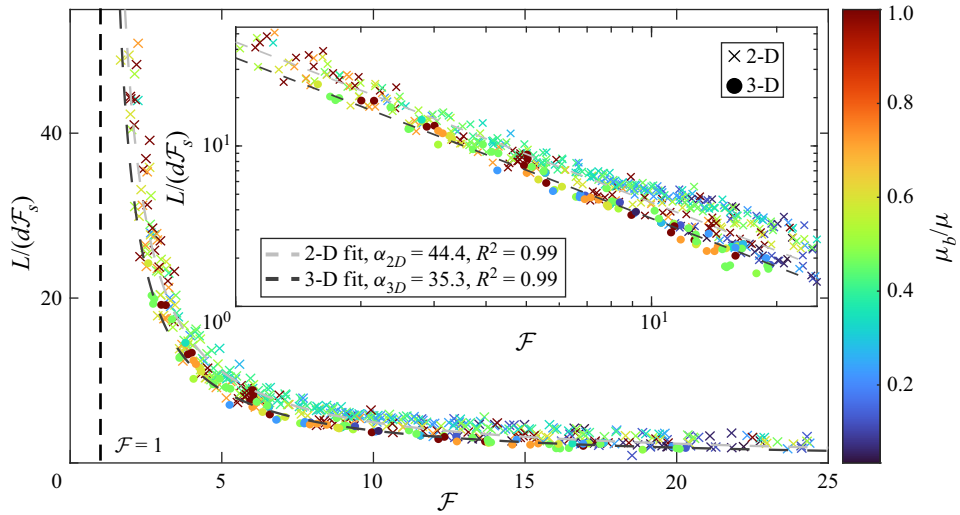


Figure 4. Scaling for the jump length using the depth-averaged Froude number \mathcal{F} based on mass hold-up and the basal Froude number \mathcal{F}_s . Here, R^2 is the coefficient of determination for the fits based on (4.1). Inset: same data in logarithmic scales.

where β is a coefficient that depends on the dimension of the system (see figure 5). This relationship can be seen as a modification of the empirical law proposed by Zhu *et al.* (2020) for granular flows down smooth inclines yet with sidewalls: in particular, see (2) in Zhu *et al.* (2020) that yields $u_s \approx \bar{u}/(h\phi/d)^{1/4}$. The latter scaling is different from (4.2) as the exponents vary, particularly the exponent for h which is negative. We do not have a clear explanation to this finding, except recalling that the present study considers unconfined flows while Zhu *et al.* (2020) were investigating confined flows with sidewalls. Nevertheless, this is an empirical way to describe the crucial interplay between apparent sliding at the smooth bottom and the granular bulk, while getting rid of the sliding velocity, which thus becomes a function of depth-averaged features (\bar{u} , h and $\bar{\phi}$) of the incoming flows. Note that the slip velocities measured in our simulations could be used in the future as a test bed for future advancement of the theory by Louge & Keast (2001). It is important to stress that the contribution of the slip velocity to depth-averaged velocity is largely dominant here for the case of a smooth incline, as depicted in figure 2 (Brodu, Richard & Delannay 2013; Faug *et al.* 2015; Zhu *et al.* 2020). This is significantly different from the case of granular flows down a rough incline with no slip velocity or negligible u_s (Louge 2003; GDRMidi 2004).

The jump length relative to the grain diameter can be predicted through the new scaling:

$$\frac{L}{d} = \gamma \bar{\phi}^{0.6} \left(\frac{h}{d}\right)^{0.4} \frac{\mathcal{F}}{\mathcal{F} - 1}, \tag{4.3}$$

where $\gamma = \alpha\beta$. The accuracy of the approach proposed in (4.3) is verified in figure 6.

4.3. Jump length–height ratio

The importance of predicting the jump length is its use in closing the augmented Bélanger equation by Méjean *et al.* (2017). In that framework, the jump length appears in the form

Length of granular jumps down inclines

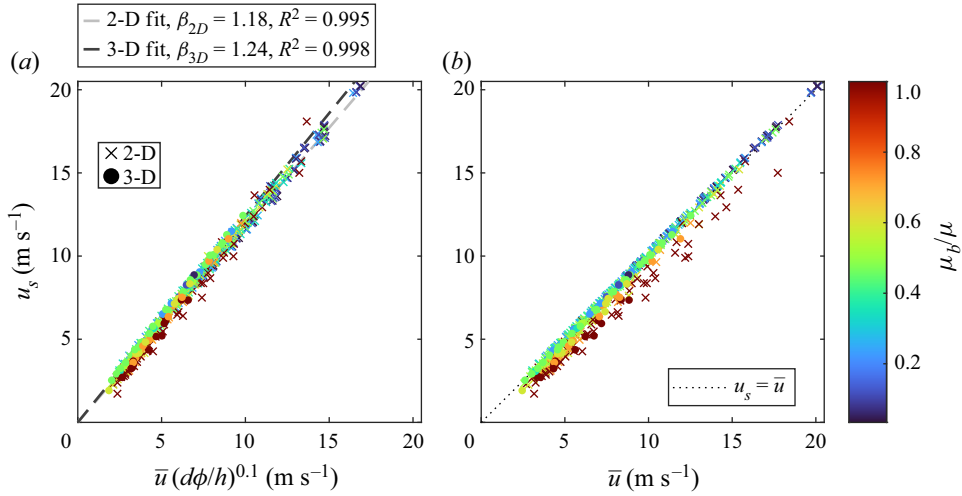


Figure 5. (a) Scaling for sliding velocity u_s considering (4.2); (b) u_s vs \bar{u} with a bigger scatter of data at higher μ_b , despite the practically apparent linear trend.

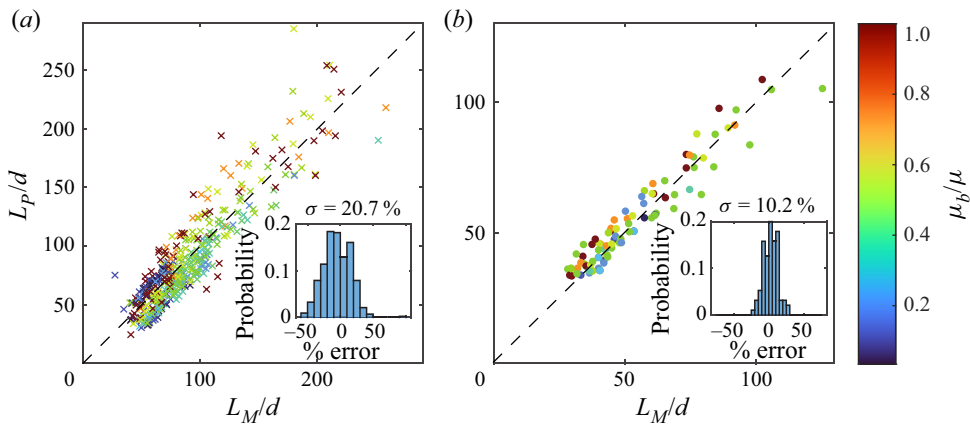


Figure 6. Predicted jump length L_P against measured jump length L_M : (a) 2-D results, (b) 3-D results. Insets are the histogram of error, defined as $2(L_P - L_M)/(L_P + L_M)$.

of the ratio L/h . By using (4.3), the ratio L/h is given by the following empirical law:

$$\frac{L}{h} = \gamma \left(\bar{\phi} \frac{d}{h} \right)^{0.6} \frac{\mathcal{F}}{\mathcal{F} - 1}. \tag{4.4}$$

Figure 7 shows the prediction of L/h using the above empirical scaling against the corresponding measured data for both the 2-D and 3-D cases. Regarding the 2-D case, some comments can be made: high values of L/h are generally obtained for higher μ_b/μ , the highest measured L/h can reach ≈ 45 , and predictions are not good for $L/h > 25$. For the 3-D system, the measured L/h values span a narrower range (≈ 6 – 15), which is less than in the 2-D case. Moreover, the trend that increasing μ_b/μ tends to generally decrease L/h is also seen (see legend colour for μ_b/μ in figure 7). The prediction of (4.4) is better and is generally very reasonable, though some data points spread away from the line of equality.

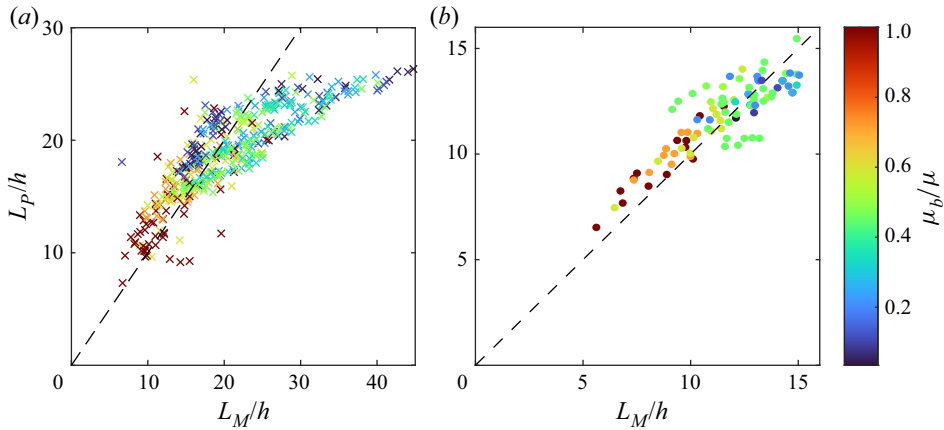


Figure 7. Predicted jump length ratio L_P/h vs measured L_M/h for 2-D (a) and 3-D (b) cases. The dashed line shows the line of equality in both plots.

5. Summary and conclusions

This work presents the results of extensive 2-D and 3-D simulations of standing jumps along inclined planes developed using the DEM. During the simulations, multiple input parameters were systematically varied to obtain a wide range of granular jump patterns. The granular flows and jumps are found to be strongly influenced by the interplay between the sliding of the first layer of grains on the base of the flow and the shearing of the granular bulk above. Plug-like incoming flows occur when there is low friction between the grains and the bottom, regardless of the interparticle friction. Increasing the bottom friction increases the shearing of the bulk until flows with Bagnold-like velocity profiles appear at high values of friction, yet with significant sliding kept at the bottom.

Concerning the length of the jump, little difference was found between 2-D and 3-D simulations as both present similar behaviours. This behaviour consists of a tendency to a constant length with increasing Froude numbers and an increasing, diverging length as the incoming flow slows down, approaching a critical regime. Despite these similarities, the overall lengths were systematically shorter in the 3-D simulations. Future works may consider studying the effective friction that controls the jump formation. This will help to quantify the amount of energy dissipated and its influence and relationship to the jump length and its final height. An empirical scaling law was proposed to determine the jump length, incorporating the sliding velocity and depth-averaged features of the incoming flows. Next, a relationship between the sliding velocity and the depth-averaged velocity was developed and encapsulated in the empirical scaling for the jump length. The obtained relationship predicts the jump length without prior knowledge of the sliding velocity, relying exclusively on depth-averaged velocity and volume fraction, flow thickness and slope inclination.

The scaling law proposed provides a closure relation for the jump length relative to the flow thickness, L/h , which is a key parameter of the augmented BÉlanger equation proposed by Méjean *et al.* (2017) to compute the jump height ratio h_*/h . Furthermore, the obtained 3-D values of L/h are found to be in the range of ≈ 6 –15, in remarkable agreement with recent laboratory measurements of jump lengths thanks to X-ray radiography: see figure 16 of Méjean *et al.* (2022). Moreover, the magnitude of the L/h ratio was found to be primarily controlled by the ratio of friction at the smooth bottom to interparticle friction (μ_b/μ), with lower L/h at high μ_b/μ . The proposed closure for L/h for 3-D granular

jumps provides engineers and designers with a more accurate way to estimate the impact of granular flows on retaining structures. Specifically, this ratio may next be used to better predict the forces that granular flows impart on retaining structures. Considering such forces would offer a promising pathway to optimize the design of more resilient retaining structures against avalanches and landslides and protecting the safety of communities and infrastructures downstream.

Supplementary material. Supplementary material is available at <https://doi.org/10.1017/jfm.2023.757>.

Funding. This work has been supported by grants from LabEx OSUG@2020 (Investissements d'avenir – ANR10 LABX56) and PHC FASIC 2022 programme (France–Australia funding).

Declaration of interests. The authors report no conflict of interest.

Author ORCIDs.

 Andrés Escobar <https://orcid.org/0000-0003-3366-9352>;

 Thierry Faug <https://orcid.org/0000-0001-6023-2549>.

REFERENCES

- ALBABA, A., LAMBERT, S. & FAUG, T. 2018 Dry granular avalanche impact force on a rigid wall: analytic shock solution versus discrete element simulations. *Phys. Rev. E* **97**, 052903.
- BRODU, N., RICHARD, P. & DELANNAY, R. 2013 Shallow granular flows down flat frictional channels: steady flows and longitudinal vortices. *Phys. Rev. E* **87** (2), 022202.
- CHANSON, H. 2009 Development of the Bélanger equation and backwater equation by Jean-Baptiste Bélanger (1828). *J. Hydraul. Engng* **135** (3), 159–163.
- FAUG, T., CHILDS, P., WYBURN, E. & EINAV, I. 2015 Standing jumps in shallow granular flows down smooth inclines. *Phys. Fluids* **27** (7), 073304.
- GDRMIDI 2004 On dense granular flows. *Eur. Phys. J. E* **14** (4), 341–365.
- GRAY, J.M.N.T. & HUTTER, K. 1997 Pattern formation in granular avalanches. *Contin. Mech. Thermodyn.* **9**, 341–345.
- GRAY, J.M.N.T., TAI, Y.-C. & NOELLE, S. 2003 Shock waves. Dead zones and particle-free regions in rapid granular free-surface flows. *J. Fluid Mech.* **491**, 161–181.
- HOOVER, W.G. & HOOVER, C.G. 2006 Smooth-particle phase stability with generalized density-dependent potentials. *Phys. Rev. E* **73** (1), 016702.
- IVERSON, R.M., GEORGE, D.L. & LOGAN, M. 2016 Debris flow runup on vertical barriers and adverse slopes. *J. Geophys. Res.* **121** (12), 2333–2357.
- JAWORSKI, A.J. & DYAKOWSKI, T. 2007 Observations of ‘granular jump’ in the pneumatic conveying system. *Exp. Therm. Fluid Sci.* **31** (8), 877–885.
- JOHANNESSON, T., GAUER, P., ISSLER, P. & LIED, K. 2009 *The design of avalanche protection dams. Recent practical and theoretical developments*. European Commission Directorate-General.
- LOUGE, M.Y. 2003 Model for dense granular flows down bumpy inclines. *Phys. Rev. E* **67** (6), 061303.
- LOUGE, M.Y. & KEAST, S.C. 2001 On dense granular flows down flat frictional inclines. *Phys. Fluids* **13** (5), 1213–1233.
- MÉJEAN, S., FAUG, T. & EINAV, I. 2017 A general relation for standing normal jumps in both hydraulic and dry granular flows. *J. Fluid Mech.* **816**, 331–351.
- MÉJEAN, S., GUILLARD, F., FAUG, T. & EINAV, I. 2020 Length of standing jumps along granular flows down smooth inclines. *Phys. Rev. Fluids* **5** (3), 034303.
- MÉJEAN, S., GUILLARD, F., FAUG, T. & EINAV, I. 2022 X-ray study of fast and slow granular flows with transition jump in between. *Granul. Matt.* **24** (26), 1–15.
- O’SULLIVAN, C. & BRAY, J.D. 2004 Selecting a suitable time step for discrete element simulations that use the central difference time integration scheme. *Engng Comput.* **21** (2/3/4), 278–303.
- POURNIN, L., LIEBLING, T.M. & MOCELLIN, A. 2001 Molecular-dynamics force models for better control of energy dissipation in numerical simulations of dense granular media. *Phys. Rev. E* **65**, 011302.
- PUDASAINI, S.P., HUTTER, K., HSIAU, S.-S., TAI, S.-C., WANG, Y. & KATZENBACH, R. 2007 Rapid flow of dry granular materials down inclined chutes impinging on rigid walls. *Phys. Fluids* **19** (5), 053302.
- SAMADANI, A., MAHADEVAN, L. & KUDROLLI, A. 2002 Shocks in sand flowing in a silo. *J. Fluid Mech.* **452**, 293–301.

- SELESNICK, I.W. & BURRUS, C.S. 1998 Generalized digital butterworth filter design. *IEEE Trans. Signal Process.* **46** (6), 1688–1694.
- SMILAUER, V., *et al.* 2021 *Yade Documentation*, 3rd edn. The Yade Project.
- SOVILLA, B., SONATORE, I., BÜHLER, Y. & MARGRETH, S. 2012 Wet-snow avalanche interaction with a deflecting dam: field observations and numerical simulations in a case study. *Nat. Hazards Earth Syst. Sci.* **12** (5), 1407–1423.
- TAI, Y.C. & LIN, Y.C. 2008 A focused view of the behavior of granular flows down a confined inclined chute into the horizontal run-out zone. *Phys. Fluids* **20** (12), 123302.
- UTILI, S., ZHAO, T. & HOULSBY, G.T. 2015 3D DEM investigation of granular column collapse: evaluation of debris motion and its destructive power. *Engng Geol.* **186**, 3–16.
- VIROULET, S., BAKER, J.L., EDWARDS, A.N., JOHNSON, C.G., GJALTEMA, C., CLAVEL, P. & GRAY, J.M.N.T. 2017 Multiple solutions for granular flow over a smooth two-dimensional bump. *J. Fluid Mech.* **815**, 77–116.
- XIAO, H., HRUSKA, J., OTTINO, J.M., LUEPTOW, R.M. & UMBANHOWAR, P.B. 2018 Unsteady flows and inhomogeneous packing in damp granular heap flows. *Phys. Rev. E* **98**, 032906.
- ZHU, Y., DELANNAY, R. & VALANCE, A. 2020 High-speed confined granular flows down smooth inclines: scaling and wall friction laws. *Granul. Matt.* **22**, 1–12.